

Ultraperipheral heavy-ion collisions in Run3 - verification of what we know or new physics?

M. Klusek-Gawenda

*Institute of Nuclear Physics Polish Academy of Sciences,
Radzikowskiego 152, PL-31-342 Kraków, Poland.*

Received 31 May 2023; accepted 28 June 2023

The theoretical predictions presented in this work are integral to the ongoing and planned experiments at RHIC and CERN-LHC laboratory. The innovation of the research lies in the possibility of making distributions of many measurable kinematic variables, which are often key to better understanding the reaction mechanism, rather than being limited to presenting only the value of the total cross section. The presented aspect of the research can be used to plan future experiments as well as to interpret already existing experimental results. The correctness of the results is strongly influenced by the type of nuclear form factor used.

Keywords: RHIC; CERN-LHC laboratory; measurable kinematic variables; reaction mechanism.

DOI: <https://doi.org/10.31349/SuplRevMexFis.4.021131>

1. Introduction

Nuclei with Ze charge moving at ultrarelativistic speed are surrounded by a strong electromagnetic field. The interaction between the nuclei is due to the exchange of photons - electromagnetic field carries. A small value of photon virtuality, $Q^2 \leq 1/R^2 \cong 800 \text{ MeV}^2$ (assuming $R = 7 \text{ fm}$), qualifies photons as quasi-real particles. In collisions of two nuclei, photon-nucleus and photon-photon collisions occur. The Equivalent Photon Approximation (EPA) in heavy-ion collisions is an approach used mainly for ultraperipheral collisions (UPC, *ang. UltraPeripheral Collisions*). As has been explored, the approximation can be successfully applied also to describe more central cases.

The equivalent photon approximation is a commonly applied method that is used to determine the probability on the production of particles that are created as a result of ultraperipheral collisions of heavy ions, Ref. [1-3]. The creators of the theory, E. Fermi, Ref. [4] and independently C. von Weizsäcker and E. Williams, Ref. [5,6] demonstrated a way to replace the electromagnetic field of a fast moving charge by the spectrum of photons.

The total cross section, expressed in impact parameter space, Fig. 1, Refs. [1,7], is given as:

$$\begin{aligned} \sigma_{A_1 A_2 \rightarrow A_1 A_2 X_1 X_2} &= \int \sigma_{\gamma\gamma \rightarrow X_1 X_2} (W_{\gamma\gamma}) N(\omega_1, \mathbf{b}_1) \\ &\times N(\omega_2, \mathbf{b}_2) S_{abs}^2(\mathbf{b}) \frac{W_{\gamma\gamma}}{2} \\ &\times dW_{\gamma\gamma} dY_{X_1 X_2} d\bar{b}_x d\bar{b}_y d^2b, \end{aligned} \quad (1)$$

where $N(\omega_i, \mathbf{b}_i)$ is the flux of photon with energy ω_i , $W_{\gamma\gamma} = M_{X_1 X_2}$ and $Y_{X_1 X_2} = (y_{X_1} + y_{X_2})/2$ are invariant mass and rapidity of the $X_1 X_2$ system. Energies of photons emitted from the nucleus and invariant mass of the pair of particles satisfy the relation:

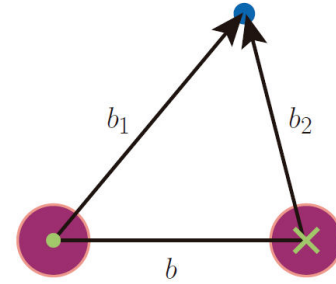


FIGURE 1. Perpendicular view in the direction of the collision of two ions. The blue point indicates the place of interaction of two photons and at the same time the place of creation of a pair of particles. Vectors \mathbf{b}_1 , \mathbf{b}_2 and \mathbf{b} specify quantities occurring in the impact parameter space. Vectors \mathbf{b}_i are hooked in the centre of the nucleus.

$$\begin{aligned} \omega_1 &= \frac{m_{t,X_1} e^{y_{X_1}} + m_{t,X_2} e^{y_{X_2}}}{2}, \\ \omega_2 &= \frac{m_{t,X_1} e^{-y_{X_1}} + m_{t,X_2} e^{-y_{X_2}}}{2}, \end{aligned}$$

$$M_{X_1 X_2}^2 = \hat{s} = 4\omega_1\omega_2 - P_{T,X_1 X_2}^2, \quad (2)$$

where

$$m_{t,X_i} = \sqrt{p_{t,X_i}^2 + m_{X_i}^2}, \quad (3)$$

is the so-called transverse mass of the particles and $P_{T,X_1 X_2}$ is the vector sum of the transverse momentum of the particles. The vector \mathbf{b}_i defines the distance between the centre of the nucleus and the photon interaction point, Fig. 2b). The implementation of the formulas in the impact parameter space is based on the relation:

$$\mathbf{b} = \mathbf{b}_1 - \mathbf{b}_2. \quad (4)$$

Additionally, in Eq. (1) the quantities \bar{b}_x and \bar{b}_y are components of the $(\mathbf{b}_1 + \mathbf{b}_2)/2$ vector:

$$\bar{b}_x = (b_{1x} + b_{2x})/2 \quad \text{and} \quad \bar{b}_y = (b_{1y} + b_{2y})/2. \quad (5)$$

$S(b)$ - the survival factor (absorption factor) depends on the impact parameter and with a good approximation can be expressed by the radius of A and B nuclei:

$$S(b) \approx \theta(b - R_A - R_B). \quad (6)$$

The absorption factor plays a key role in the UPC, as it excludes cases where nuclei break up as a result of their collision. The photon flux, $N(\omega, b)$, appearing as a primary component of the EPA model, Refs. [1, 8], is expressed by the nuclear form factor, $F(q^2)$, which depends on the photon virtuality:

$$N(\omega, b) = \frac{Z^2 \alpha_{em}}{\pi^2} \frac{1}{b\omega} \times \left| \int du u^2 J_1(u) \frac{F\left(\frac{(\frac{\omega b}{\gamma})^2 + u^2}{b^2}\right)}{\left(\frac{\omega b}{\gamma}\right)^2 + u} \right|^2. \quad (7)$$

Here, γ is the Lorentz factor. Treating the nucleus as a point charge, the photon flux is expressed by a modified Bessel function of the second kind:

$$\frac{d^3 N(\omega, b)}{d\omega d^2 r} = \frac{Z^2 \alpha_{em} X^2}{\pi^2 \omega \gamma^2} K_1^2(X), \quad (8)$$

where ω is the energy of emitted photon, b - distance between a photon and the centre of the emitting nucleus in the impact parameter space, and the $X = b\omega/\gamma$ parameter takes relativistic effects into account. The analyses were performed for the most realistic description of the nucleus by applying the Fourier transform of the charge distribution:

$$F_{real}(q^2) = \frac{4\pi}{q} \int \rho(r) \sin(qr) r dr. \quad (9)$$

The two-parameter Fermi distribution (also called the Woods-Saxon charge distribution), Ref. [9], is normalized to the atomic number.

2. Light-by-light scattering

In Maxwell's classical theory, photons do not interact with each other, *i.e.* no $\gamma\gamma \rightarrow \gamma\gamma$ type process can occur. At the classical level, two electromagnetic waves in vacuum overlap and pass through each other without scattering. Already in 1933 it was suggested, Ref. [10], that virtual electron-positron pairs are the source of photon-photon scattering. Further analysis led to the Euler-Kockel-Heisenberg Lagrangian, which modifies the classical Maxwell equations in vacuum by nonlinear conditions, Ref. [11]. Quantum theory states that γ -quanta can interact through quantum fluctuations. Elastic light-by-light scattering in LO and NLO has

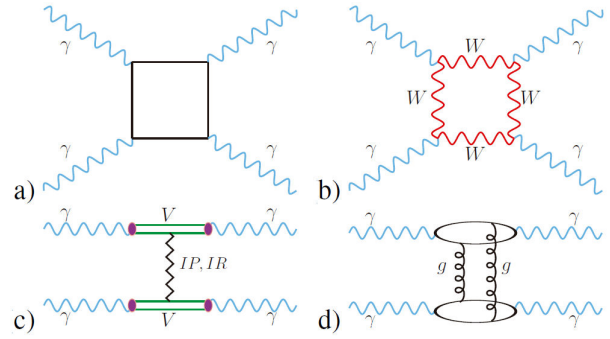


FIGURE 2. Light-by-light mechanisms. a) Lepton and quark loop, b) W boson exchange loop (spin 1), c) VDM-Regge mechanism and d) two-gluon exchange.

has been discussed many times in the literature, Ref. [12-14], while it has never been measured experimentally before (before the date of the theoretical analysis, *i.e.* 2016). For example, in e^+e^- collisions, the energy of the subprocess as well as the photon to electron coupling is relatively small, so the corresponding cross section is difficult to measure. The enhancement of the cross section by the charge of heavy ions ($\propto Z_1^2 Z_2^2$) gave a premise for the possibility to obtain optimistic predictions.

Performing a comprehensive analysis of the process requires consideration of as many mechanisms as possible that contribute to a given final state. Predictions for nuclear light-by-light scattering have considered contributions from:

- Fermionic loop, Fig. 2a). The amplitude for the so-called boxes was calculated using the FormCalc software [15] and the LoopTools library [16] in Mathematica. The grid for the given photon polarization vectors, taking into account the four-momentum of incoming and outgoing photons, was used to determine the elementary cross section, $\gamma\gamma \rightarrow \gamma\gamma$. The obtained result for the lowest order QED mechanism is identical to the distributions determined by other methods, Refs. [13,14,17]. Including the QCD and QED corrections (two-loop Feynman diagrams), Ref. [14], in the ultrarelativistic approximation ($|\hat{s}|, |\hat{t}|, |\hat{u}| \gg m_f^2$) gives a small numerical correction compared to the main contribution.
- Loop with W^\pm boson exchange, Fig. 2b), Ref. [18].
- VDM-Regge (*Vector Dominance Model*), Fig. 2c), Ref. [19]. Both photons in the initial state fluctuate to a virtual vector meson (three light mesons are considered, $i, j = \rho, \omega, \phi$). The interaction between photons occurs only when each photon is in one of the three considered hadronic states. The characteristic parameters for the VDM-Regge model were determined using the standard Regge factorization and the Donnachie-Landshoff parameterization, Ref. [20-22].

- Two-gluon exchange, Fig. 2d), Ref. [23]. The three-loop mechanism considers 16 diagrams that differ in the configuration of gluon coupling to a given loop. The amplitude defined in the interaction coefficient representation, \mathcal{J} , Ref. [24,25], depends on the transverse momentum transfer \mathbf{q} . The parametrization of the momentum loop has occurred such that the gluons carry a transverse momentum $\mathbf{q}/2 \pm \kappa$.
- The decay of resonances, Fig. 2f), Ref. [26].

The first measurement of two photon production was made in ultraperipheral heavy ion collisions. The ATLAS group made the first experimental verification, Ref. [27], a theory predicted more than 80 years ago, Ref. [28]. Experimental distributions of invariant mass and acoplanarity are compared with results determined according to the theoretical model presented in Sec. 2 (red lines in Fig. 2). Comparison of theoretical and experimental total cross sections taking into account experimental cuts, *i.e.* $M_{\gamma\gamma} > 6$ GeV, $p_{t,\gamma} > 3$ GeV, $|\eta_\gamma| < 2.4$, $P_{t,\gamma\gamma} < 2$ GeV, $A_{co} < 0.01$, looks as follows:

$$\sigma_{PbPb \rightarrow PbPb\gamma\gamma}^{\text{theory}} = 51 \pm 0.02 \text{ nb} ,$$

$$\sigma_{PbPb \rightarrow PbPb\gamma\gamma}^{\text{ATLAS/2017}} = 70 \pm 20 \text{stat.} \pm 17 \text{syst. nb} ;$$

Ref. [30] ,

$$\sigma_{PbPb \rightarrow PbPb\gamma\gamma}^{\text{ATLAS/2019}} = 78 \pm 13 \text{stat.} \pm 7 \text{syst.} \pm 7 \text{lumi. nb} ;$$

Ref. [31].

Subsequent measurements were associated with higher statistics and extension of the invariant range: $\sigma_{PbPb \rightarrow PbPb\gamma\gamma}^{\text{theory}} = 103 \pm 0.034 \text{ nb}$ vs $\sigma_{PbPb \rightarrow PbPb\gamma\gamma}^{\text{CMS}} = 120 \pm 46 \text{stat.} \pm 28 \text{syst. nb}$ [30], $\sigma_{PbPb \rightarrow PbPb\gamma\gamma}^{\text{theory}} = 80 \pm 0.033 \text{ nb}$ vs $\sigma_{PbPb \rightarrow PbPb\gamma\gamma}^{\text{ATLAS/2020}} = 120 \pm 17 \text{stat.} \pm 13 \text{syst. nb}$ [31].

Current experimental capabilities allow the measurement of light-by-light scattering in the UPC for the invariant mass range $M_{\gamma\gamma} > 5$ GeV, Ref. [30,31]. Below this limit, in addition to fermion diagrams, the decay of η , $\eta'(958)$, $\eta_c(1S)$, $\eta_c(2S)$, $\chi_{c0}(1P)$ resonances plays a non-negligible contribution to the $\gamma\gamma$, Ref. [26]. The amplitude of the $\gamma\gamma \rightarrow R \rightarrow \gamma\gamma$ process for the resonance in the s channel was determined according to the formula discussed in Ref. [32]. Although the inclusion of resonances in t and u channel leads to a broad continuum, these contributions are several orders of magnitude smaller than the contribution for channel s , Ref. [26]. The masses and decay widths of pseudoscalar and scalar mesons were taken from PDG [33].

A completely new issue, not previously considered in the literature, was the consideration of the pionic background from the $\gamma\gamma \rightarrow \pi^0(\rightarrow \gamma\gamma)\pi^0(\rightarrow \gamma\gamma)$ process, where the measurable photon comes from the decay of another pion, Ref. [34]. An excellent description of the Belle [35] and

Crystall Ball [36] data for the $\gamma\gamma \rightarrow \pi^0\pi^0$ process is given in Ref. [32]. The correctness of the data description is based on the consideration of nine resonances, meson exchange in the t -channel and the so-called pQCD contributions. The results of the analysis carried out, Ref. [32], are the only correct interpretation of the data for the production of a pair of charged and neutral pions in the full energy range. The nuclear calculations were based on the calculation of the dense three-dimensional grid in the rapidity of each pion and its transverse momentum, Eq. (10). The radiative decays of both pions were considered in the Monte Carlo code. The pions are mesons with spin 0, so the decay was treated as an isotropic decay in the rest system of the decaying pion. The kinematic distributions of the photons were defined by transforming the variables to the photon laboratory system (nucleus-nucleus centre-of-mass system). Different kinematic cuts were applied to the photons to extract the possibility of measuring a pure signal.

Predictions targeting Run3@LHC have been made for the acceptance of the two-photon state measurement, taking into account the energy resolution of the measurement. The possibility of two photons detection in central rapidity for the ALICE experiment ($|\eta_\gamma| < 0.9$ and $E_{t,\gamma} > 0.2$ GeV), Ref. [37], and in the so-called forward direction for the LHCb experiment ($2 < \eta_\gamma < 4.5$ and $E_{t,\gamma} > 0.2$ GeV). For the measurement of photons in ALICE, the electromagnetic calorimeters EMCal and PHOS or the photon conversion method (PCM) are used. Photons transform into e^+e^- pairs and are reconstructed by detecting the tracks of two leptons. The advantage of electromagnetic calorimeters is their high capability, but unfortunately they have a limited range of solid angle. Measurement with the PCM covers the full solid angle, but has a reduced efficiency. The possibility of a hybrid measurement was assumed, in which one photon is detected by the calorimeter and the other is reconstructed by the PCM. For ALICE, the energy resolution was set to a level of $\sigma_{E_\gamma}/E_\gamma = 1.3\%$ and in the case of the LHCb experiment a parameterization was used, Ref. [38]:

$$\frac{\sigma_{E_\gamma}}{E_\gamma} = \frac{0.085}{\sqrt{E_\gamma}} + \frac{0.003}{E_\gamma} + 0.008 , \quad (10)$$

where E_γ is the energy of a single outgoing photon. It should be emphasized that for a massless particle, $p_{t,\gamma}$ and $E_{t,\gamma}$ kinematic variables are identical. Similar relation is observed between rapidity and pseudorapidity of the photon.

A summary of the contributions to the $\gamma\gamma$ state that come from fermion loops, meson decays and the pionic background, Table I, shows that the largest cross section occurs for the production of the η resonance. Although the contribution coming from the pionic background exceeded the fermion signal (in the range up to $M_{\gamma\gamma} = 2$ GeV), with sufficiently good measurement statistics, it is possible to measure the signal coming from the η meson. Above the limit, $M_{\gamma\gamma} = 2$ GeV, the unwanted two-pionic background is no longer a leading contributor to the total cross section. The prediction phase space was limited to $M_{\gamma\gamma}^{\text{max}} = 5$ GeV. The

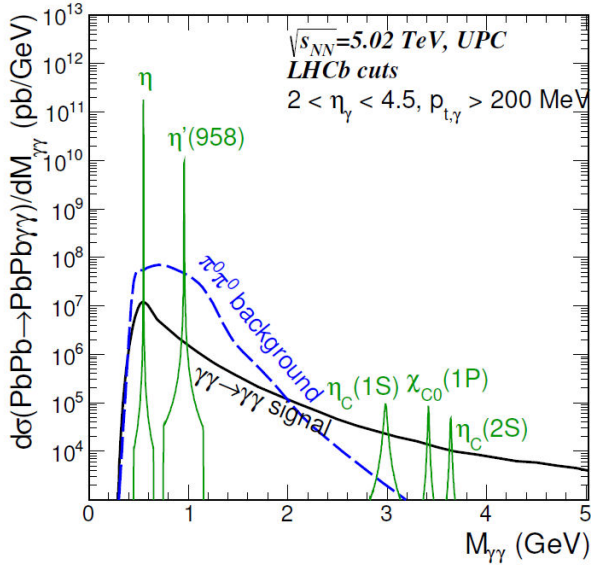


FIGURE 3. Differential cross section as a function of a photon pair invariant mass. Predictions were made for the indicated kinematic cuts: $2 < \eta_\gamma < 4.5$ and $p_{t,\gamma} > 0.2$ GeV. Results with energy resolution parametrization, Eq. (10). “Boxed” signal - black solid line, two-pionic background - blue dashed lines, meson decay - solid green line.

TABLE I. Total nuclear cross section in [nb] for ultraperipheral Pb-Pb collisions at energy $\sqrt{s_{NN}} = 5.02$ TeV.

Energy Kinematic cutting	$W_{\gamma\gamma} = (0 - 2)$ GeV		$W_{\gamma\gamma} > 2$ GeV	
	ALICE	LHCb	ALICE	LHCb
boxes	4 890	3 818	146	79
to $\pi^0\pi^0$	135 300	40 866	46	24
η	722 573	568 499	-	-
$\eta'(958)$	54 241	40 482	-	-
$\eta_c(1S)$	-	-	9	5
$\chi_{c0}(1P)$	-	-	4	2
$\eta_c(2S)$	-	-	2	1

determination of the split results presentation at $M_{\gamma\gamma} = 2$ GeV arose from the desire to reduce the background in the invariant mass range, where it dominates.

The mass distributions of the invariant photon pair, taking into account the kinematic constraints of ALICE and LHCb, are similar in normalization and shape. Two distinct peaks originating from the decay of the η and η' meson are observed, Fig. 3. Above $M_{\gamma\gamma} = 2$ GeV there will be a possibility to detect two photons, which will come from a pure signal and should not be disturbed by the pionic background. Taking into account the energy resolution does not change the total cross section, but results in a reduction of the maximum value of the distributions, Fig. 3b). The effect is clearly visible for low-energy resonant contributions.

Appropriate signal correlations were introduced to reduce the pionic background, which were quantified using scalar and vector asymmetry:

$$A_S = \frac{|\mathbf{p}_{t,\gamma_1}| - |\mathbf{p}_{t,\gamma_2}|}{|\mathbf{p}_{t,\gamma_1}| + |\mathbf{p}_{t,\gamma_2}|}, \quad A_V = \frac{|\mathbf{p}_{t,\gamma_1} - \mathbf{p}_{t,\gamma_2}|}{|\mathbf{p}_{t,\gamma_1} + \mathbf{p}_{t,\gamma_2}|}. \quad (11)$$

The formalism used assumes that $\mathbf{p}_{t,\gamma_1} = \mathbf{p}_{t,\gamma_2}$. The scalar asymmetry, A_S , is a measure of the relative difference in the transverse momenta of the photons. Due to the finite value of the energy resolution, the value of A_S is non-zero for two oppositely directed photons. The vector asymmetry reflects the convolution of the experimental energy resolution and the azimuthal angle measurement. The implementation of an azimuthal angle resolution of 2% allows for a quantitative representation of the correlation of the two defined asymmetries. The results for the signal, Fig. 3a), and for the pionic background, Fig. 3b), show the relation: $A_V > A_S$. The distribution for photon background pairs derived from $\pi^0\pi^0$ decays is an order of magnitude broader compared to the signal distribution. Careful selection of constraints on the asymmetry parameters results in a significant reduction of the background and an increase in the signal-to-background ratio, while negligibly changing the signal.

The signal is extracted by using the scalar asymmetry as the separation variable. Normally, a one- or two-dimensional distribution of signal and background, Fig. 4a), is fitted to the intervals of the separation variable and successively transformed to a distribution in another measurable quantity. Here the one-dimensional analysis is based on the mass distribution of an invariant photon pair, Fig. 4b). The separation variable is divided into three independent areas: $A_S = (0, 0.02)$, $(0.02, 0.04)$, $(0.04, 0.06)$, which are marked in red, green and grey in Fig. 4a), respectively. The signal area defined by the interval $0 < A_S < 0.02$ contains about 95% of the events originating from the signal. The remaining 5% is distributed in further areas of scalar asymmetry. At the same time, less than 10% of the pionic background is concentrated in the first A_S interval. The reduction of the background at the limit $0 < A_S < 0.02$ is indisputably noticeable in the invariant mass distribution of the two photons, Fig. 4b). However, although the considered cut has reduced the background by a factor of 10 this contribution still dominates in the invariant mass range $M_{\gamma\gamma} < 2$ GeV. Extracting the signal in the mass range where the largest background cross section appears, *i.e.* $M_{\gamma\gamma} \approx 1.2$ GeV, is possible using the multidimensional *sideband subtraction* method, Ref. [38]. The quantitative results of signal efficiency and background suppression are dependent on the statistics data available in the analysis. Analogous calculations can be performed as a function of the rapidity or transverse momentum of a single photon.

The theoretical analysis of the light-by-light scattering, Refs. [19,23,34], has been extended to include the predictions for Run3&Run4ⁱ@LHC, Ref. [39]. Summary of distributions for lead-lead ($\sqrt{s_{NN}} = 5.52$ TeV) and argon-argon collisions ($\sqrt{s_{NN}} = 6.3$ TeV) with planned acceptance parameters indicates real possibility to measure photon signal in the range of invariant mass: $M_{\gamma\gamma} = (2 - 5)$ GeV. In the

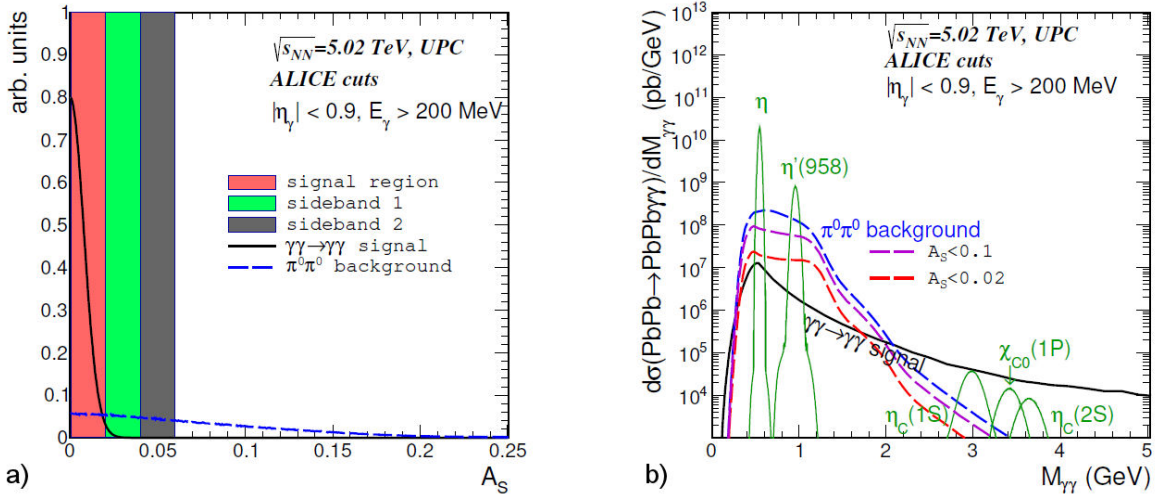


FIGURE 4. a) Distribution of scalar asymmetry of signal and pionic background. b) Distribution of invariant mass of two photons with limitation on scalar symmetry. Signal - solid line, two-pionic background - dashed lines.

case of $Ar - Ar$ collisions, the cross sections are about two orders of magnitude smaller than those predicted for $Pb - Pb$ collisions. This is a direct result of smaller electric charge of argon nucleus, $Z_{Pb}/Z_{Ar} \approx 430$. Assuming dedicated luminosity for $Ar - Ar$ collisions in the range $L = (3 - 8.8) \text{ pb}^{-1}$, one obtains possibility of 1460 – 4280 events for ALICE experiment and 11 – 34 events for LHCb. The estimation concerns the invariant mass range, where the two-pionic background does not play an important role, *i.e.* $M_{\gamma\gamma} > 2$ GeV.

3. Four-lepton productions

The production of two electron pairs in ultraperipheral heavy ion collisions was studied in full phase space, *i.e.* without imposing a limitation on kinematic variables, Ref. [40]. Formalism taking into account the integral over the impact parameter allows determining the value of the total cross section and the distribution of the impact parameter. The significant cross section comes from small values of the transverse momentum of the lepton. Unfortunately, such small $p_{t,e}$ cannot be measured with available detectors. The presented analysis, Ref. [41], represents the first description of the production of double scattering of two electron-positron pairs in a UPC including kinematic restriction dictated by experimental requirements. The aim of the study was to make predictions that are likely to be verified experimentally at the LHC. It is worth mentioning that so far no double scattering mechanism has been verified in ultraperipheral heavy ion collisions.

Before performing calculations for the production of two electron-positron pairs, the formalism defined in Eq. (9) was verified by comparing theoretical results with experimental ALICE data, Ref. [42], for the $PbPb \rightarrow PbPbe^+e^-$. The theoretical result, based on the equivalent photon approximation, correctly describes the available experimental data, Fig. 5. The implemented lowest order of the QED perturbation calculus seems to be sufficient and no higher order cor-

rections are necessary. Corrections from the Coulomb effect have been discussed many times, Refs. [43-48]. However, the analysed models have not taken into account the possibility of imposing experimental limitation, which is a key aspect of the research. The situation looks even more complicated for double scattering. The problem should be returned to when the first data for the $A_1A_2 \rightarrow A_1A_2\ell^+\ell^-\ell^+\ell^-$ process appears.

After a successful verification of the theoretical model for the electron-positron pair production, calculations were performed for the production of double scattering of e^+e^- two pairs, Ref. [41]. Table II contains the number of events for the $PbPb \rightarrow PbPbe^+e^-e^+e^-$ process at $\sqrt{s_{NN}} = 5.5$ TeV

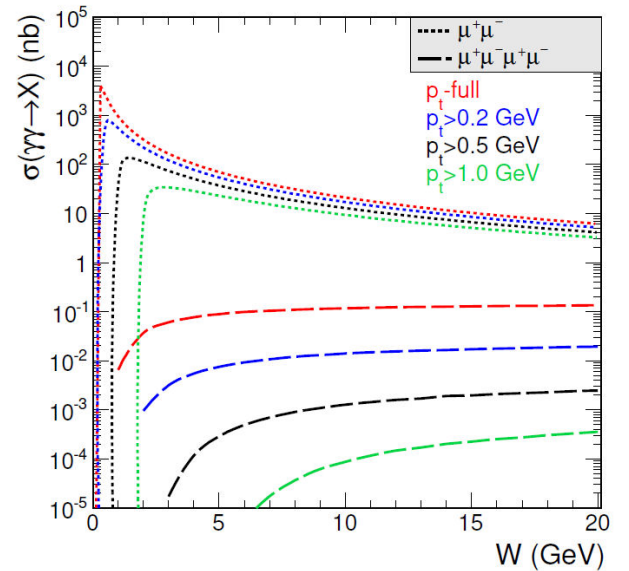


FIGURE 5. Elementary cross section for the production of two (dotted line) and four muons (dashed line). Results for the muon transverse momentum are shown with different conditions on the phase space: $p_{t,\mu} > 0, 0.2, 0.5$ and 1 GeV.

TABLE II. Number of events for the $PbPb \rightarrow PbPbe^+e^-e^+e^-$ process at collision energy $\sqrt{s_{NN}} = 5.5$ TeV. Results are given for different cuts on the rapidity and transverse momentum of a single electron/positron. Assumed: $L = 1 \text{ nb}^{-1}$. Results are from the Ref. [41].

Limitation	Nevents
$p_{t,e} > 0.2 \text{ GeV}$	52 525
$p_{t,e} > 0.2 \text{ GeV}, y_e < 2.5$	10 636
$p_{t,e} > 0.2 \text{ GeV}, y_e < 1$	649
$p_{t,e} > 0.3 \text{ GeV}, y_e < 4.9$	7 447
$p_{t,e} > 0.3 \text{ GeV}, y_e < 2.5$	2 052
$p_{t,e} > 0.5 \text{ GeV}, y_e < 4.9$	704
$p_{t,e} > 0.5 \text{ GeV}, y_e < 2.5$	235
$p_{t,e} > 1.0 \text{ GeV}$	25
$p_{t,e} > 1.0 \text{ GeV}, y_e < 4.9$	23
$p_{t,e} > 1.0 \text{ GeV}, y_e < 2.5$	10
$p_{t,e} > 1.0 \text{ GeV}, y_e < 1$	1

collision energy. Results are given for different kinematic limits imposed by the ALICE, ATLAS and CMS experiments. For example, the ALICE main detector allows identification of particles practically from $p_{t,e} > 0.2 \text{ GeV}$. ATLAS detector measures leptons in the rapidity range: $|y_e| < 2.5^{ii}$ and with the limit: $p_{t,e} > 0.5 \text{ GeV}$. As a final results, the statistics of the event collected by ALICE are ~ 45 larger than those calculated for the ATLAS detector conditions. The number of particles decreases drastically with a higher limitation on the given kinematic variables. However, it does not change the fact that even a detector with relatively narrow rapidity range ($|y_e| < 2.5$) and $p_{t,e} > 0.3 \text{ GeV}$ could make the first measurements of the four-lepton state ($e^+e^-e^+e^-$) in the UPC with a successful detection of more than 2000 cases (assuming the value of luminosity: $L = 1 \text{ nb}^{-1}$).

The cross section for the leptons production is strongly dependent on the collision energy, Fig. 5. At relativistic energies, $\sqrt{s_{NN}} = 50 \text{ GeV}$, the cross section for production of two electron-positron pairs is of the order of 1 nb for the cutoff $p_{t,e} > 0.3 \text{ GeV}$ and 20 orders smaller for cutoff $p_{t,e} > 2 \text{ GeV}$. That is, the larger $p_{t,e}^{min}$, the greater the difference in the cross sections for the production of one and two e^+e^- pairs. This drastic difference becomes blurred for ultrarelativistic collisions of heavy ions ($\sqrt{s_{NN}} \geq 100 \text{ GeV}$). Both cross section increase rapidly with increasing collision energy. However, the result for the double scattering mechanism increases faster than for single photon fusion. A similar effect was also observed for $c\bar{c}c\bar{c}$ production in proton-proton collisions, Ref. [49].

A potential background for the process under consideration is the production of four charged pions. The $\pi^+\pi^-$ pairs may originate from the decay of two $\rho^0(770)$ mesons formed as a result of two-photon fusion, Ref. [7], as well as from the double scattering mechanism of the

$\rho^0(770)$ meson, Ref. [50]. By equating the four-pionic contribution (derived from the vector meson photoproduction) to the $e^+e^-e^+e^-$ production, it was found that the total cross section depends very strongly on the limit on the transverse momentum of the particle. The ratio of the cross sections $\sigma(PbPb \rightarrow PbPbe^+e^-e^+e^-)/\sigma(PbPb \rightarrow PbPb\pi^+\pi^-\pi^+\pi^-)$ for given limits on transverse momentum, looks as follows: $p_t^{min} = 0.3 \text{ GeV} \rightarrow 0.2\%$, $p_t^{min} = 0.5 \text{ GeV} \rightarrow 8\%$. The greater p_t^{min} value, the greater the chance of measuring four leptons. Knowing contributions from the pionic background, it seems possible to remove this “unwanted” contribution by an appropriate selection of variables.

The performed analysis, Ref. [41], showed that at a sufficiently high luminosity value, it seems possible to measure for the first time the double scattering process of two electron-positron pairs in UPC. Detection of two electrons or two positrons (particles with the same charge) would already be a clear signal of the double scattering mechanism. Therefore, it was valuable to analyse the distribution of the rapidity distance of two out four produced leptons, $y_{diff} = y_{e^+} - y_{e^-}$ or $y_{diff} = y_{e^\pm} - y_{e^\pm}$. The distributions for a pair with the same charge have a wider distribution regardless of the limit on the transverse momentum of the lepton. It is assumed that electron and positron created from the same scattering have the same values of transverse momentum. By imposing a restriction to exclude back-to-back production cases, one can expect to measure electron/positron coincidences from different scattering. Similarly, making predictions for triple scattering is possible, but the cross section will be suppressed by several orders of magnitude.

The lepton scattering analysis was also performed for two muon pairs, Ref. [51]. The results are compared with a mechanism not yet considered in the literature - four leptons direct production, Fig. 6b). The distributions for the elementary cross section, $\gamma\gamma \rightarrow \mu^+\mu^-\mu^+\mu^-$, were determined by using the power of KATIE [52] and the AVHLIB library [53]. The event generator in general is intended for processes in which the initial states (here photons) have a clear dependence in the transverse momentum. The implementation of several corrections has made it possible to move from hadron scattering (at the parton level) to a scattering model for photons, which are treated as particles on a mass shell. The amplitude of the process with four particles in the final state was calculated numerically using recursive methods, thus keeping the computational complexity under control, Ref. [51]. The $\sigma(\gamma\gamma \rightarrow \mu^+\mu^-\mu^+\mu^-; W)$ grid obtained with the generator, taking into account the limit on the transverse momentum of a single muon, was implemented into a code calculating the nuclear cross section in UPC in the impact parameter space.

The single scattering mechanism is understood as a direct creation of particles in $\gamma\gamma$ fusion. Comparison of total elementary cross sections for $\gamma\gamma \rightarrow \mu^+\mu^-$ and $\gamma\gamma \rightarrow \mu^+\mu^-\mu^+\mu^-$ processes shows dependence on the value of p_t^{min} , Fig. 5. For production of one pair of muons, the value of the cut on transverse momentum of the lepton is signifi-

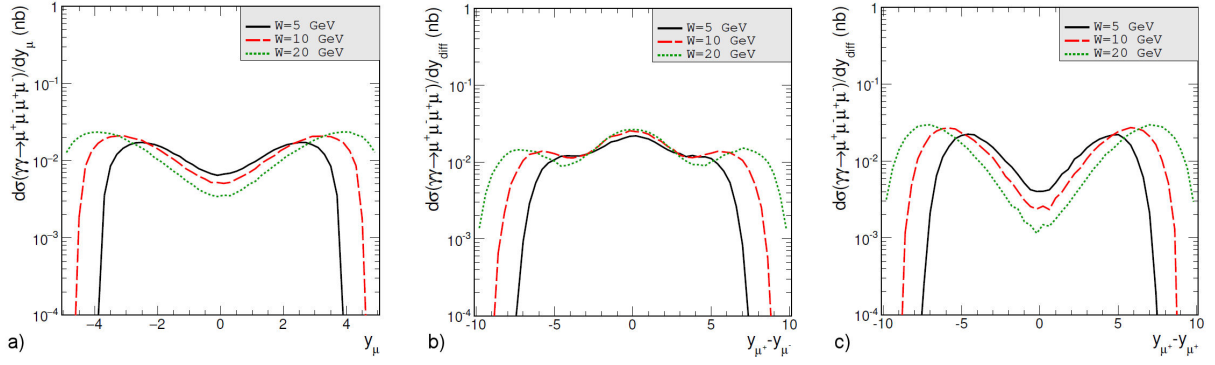


FIGURE 6. Differential cross section for the $\gamma\gamma \rightarrow \mu^+\mu^-\mu^+\mu^-$ process. a) Rapidity, b) difference in rapidity of muon of opposite charge and c) difference in rapidity of muons of the same sign are shown for a fixed energy value, $W_{\gamma\gamma} = 5, 10, 20$ GeV, solid, dashed and dotted line respectively.

cant at small values of $W_{\gamma\gamma}$. For production of four muons, the bigger value of p_t^{min} , the smaller cross section in the whole energy range. At the same time, it should be noted that the cross section for production of a single pair of muons is about ten times larger at $W_{\gamma\gamma} = 20$ GeV and at least four orders of magnitude larger for lower energy values compared to $\sigma_{\gamma\gamma \rightarrow \mu^+\mu^-\mu^+\mu^-}$.

The direct production of two muon pairs is a new mechanism that has never been analysed before. Muon rapidity distribution, Fig. 6a), clearly shows that muons originating from the four-body final state, Ref. [51], are predominantly produced in the forward/backward direction. The spectrum broadens with increasing energy. With increasing value of $W_{\gamma\gamma}$, the maximum of the distribution shifts towards larger values of rapidity. It follows that the muon scattering angle increases for higher energies. From the distribution in the difference of muon rapidity [particles with the same, Fig. 6b), and opposite sign of charge, Fig. 6c)], respectively) it is deduced, that the maximal value of the probability of production of four muons is in the case, when muons μ^+ and μ^- are moving exactly in opposite directions in a perpendicular plane and muons of the same charge sign move in the same direction at large rapidity distances.

The analysis of the production of four leptons via the double scattering mechanism, Fig. 6c), Ref. [41], has been extended to include results for muons, Ref. [51]. A qualitative comparison of the cross sections was performed using the invariant mass distribution of four muons, Fig. 6a). By imposing a limit on the transverse momentum of each muon, one notices a strong dependence on the value of cuts independently of the considered production mechanism of $\mu^+\mu^-\mu^+\mu^-$. Since the result for double scattering production, $\gamma\gamma \rightarrow \mu^+\mu^- \otimes \gamma\gamma \rightarrow \mu^+\mu^-$ (DS, double scattering), turns out to be unbeatable, the first experimental measurement of four leptons produced as a result of an ultraperipheral collision of heavy ions should not include cases coming from the single scattering process, $\gamma\gamma \rightarrow \mu^+\mu^-\mu^+\mu^-$ (SS, single scattering). In addition, the distribution of the rapidity difference, Fig. 7b), shows a strong correlation of muons coming from the same scattering, *i.e.*, muons with opposite charge

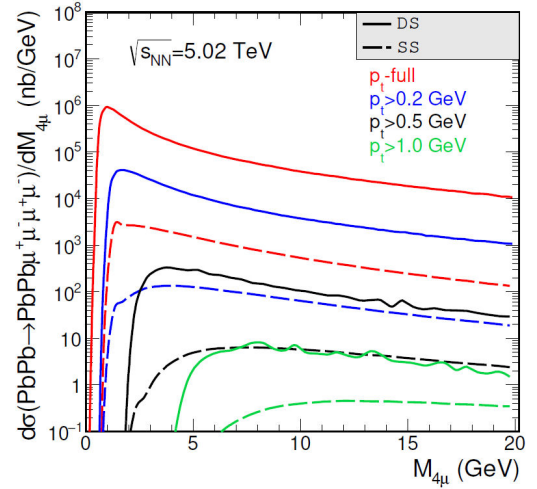


FIGURE 7. Nuclear differential cross section as a function of invariant mass of four muons. Comparison of contributions for the mechanism of production of one pair of muons (legend: $\mu^+\mu^-$), two pairs of muons coming from single scattering (legend: SS) and from double scattering (analogously as it was done for the production of two pairs of e^+e^- ; legend: DS). Collision energy: $\sqrt{s_{NN}} = 5.02$ TeV.

signs. The corresponding distribution for these cases reaches maximum in $y_{diff} = y_{\mu^+} - y_{\mu^-} = 0$. No similar correlation is expected for muons of the same sign. The cross section for the production of one muon pair is about three orders of magnitude larger than for the creation of four muons coming from the double scattering mechanism. It was not possible to show the distributions in y_{diff} for the direct production of four leptons (SS). This is due to the organization of nuclear calculations and the method of determining the elementary cross section, Eq. (11). The map prepared with the KATIE generator determined the dependence of the cross section on the energy for a fixed limitation on the muon transverse momentum. Preparation of a more detailed, multidimensional map, which could be used to determine the nuclear cross section e.g. as a function of differential rapidity, was beyond the scope of the performed analysis. This fact seemed justified given the following comparison:

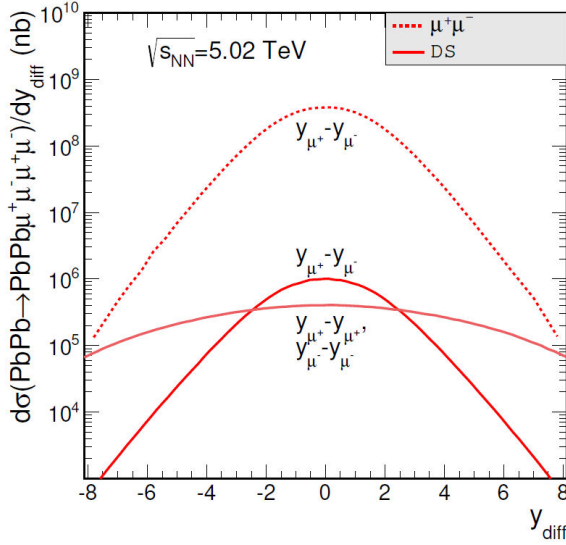


FIGURE 8. Nuclear differential cross section as a function of differential rapidity. Comparison of contributions for the mechanism of production of one pair of muons (legend: $\mu^+\mu^-$), two pairs of muons coming from single scattering (legend: SS) and from double scattering (analogously as it was done for the production of two pairs of e^+e^- ; legend: DS). Collision energy: $\sqrt{s_{NN}} = 5.02$ TeV.

$$\sigma_{A_1 A_2 \rightarrow A_1 A_2 (\mu^+ \mu^-) (\mu^+ \mu^-)} / \sigma_{A_1 A_2 \rightarrow A_1 A_2 \mu^+ \mu^- \mu^+ \mu^-} \approx (10^2 - 10^3),$$

$$\sigma_{A_1 A_2 \rightarrow A_1 A_2 \mu^+ \mu^-} / \sigma_{A_1 A_2 \rightarrow A_1 A_2 (\mu^+ \mu^-) (\mu^+ \mu^-)} \approx (10^2 - 10^3).$$

The last result is also true for electron-positron pair/pair production. It is worth mentioning that for a relatively small limit on the value of the transverse momentum of the lepton, $p_{t,\ell} > 0.5$ GeV, the nuclear cross section is the same for electrons and muons. Distributions for $\tau^+\tau^-$ pair production indicated similar coincidence at $p_{t,\ell}^{\min} > 4$ GeV. Presented analyses for leptons production consider $\gamma\gamma \rightarrow \ell^+\ell^-$ LO QED. The correctness of this choice is justified by the agreement of theoretical results with experimental data, *i.e.* the $PbPb \rightarrow PbPbe^+e^-$ process with data of the ALICE group [42] and the $PbPb \rightarrow PbPb\mu^+\mu^-$ process with data from the ATLAS group [54].

4. Summary

The theoretical predictions presented in this work are an integral part of the ongoing and planned experiments at RHIC and CERN-LHC laboratory. The innovation of the research lies in the possibility of making distributions of many measurable kinematic variables, which are often key to better understanding the reaction mechanism, rather than being limited to presenting only the value of the total cross section. The presented aspect of the research can be used to plan future experiments as well as to interpret already existing experimental results. The correctness of the results is strongly

influenced by the type of nuclear form factor used, which is known to scatter electrons on nuclei. The use of a simplified monopole form factor gives about 10% larger total cross sections. For high rapidity and large transverse momenta of the objects produced, the effects can be even larger. Application of the Fourier transform of the charge density in the nucleus allows obtaining a result, which is more consistent with existing experimental data. Although the inclusion of the aforementioned transform in the model is somewhat more difficult - the presented theoretical results take into account the realistic charge distribution in the nucleus.

The differential distributions of the produced particles were determined from multi-dimensional integrals. The basic EPA formulation, in impact parameter space, contains six integration variables. Taking into account the full kinematics of the process, *i.e.* transformation to momentum space, requires taking into account even four additional dimensions.

A landmark paper discussing the possibility of the first measurement of light-by-light scattering, Ref. [19], showed that from a theoretical point of view it becomes possible and instructive to measure a photon pair for the ultraperipheral case, *i.e.*, when the nuclei collide at a distance larger than the sum of their geometric radii. One of the key elements of the analysis was the correct determination of the elementary cross section for mechanisms with quark and lepton loops and the modification of the formulas for the nuclear cross section to take into account the experimentally available phase space. A contribution from, not considered in this context, is also shown, VDM-Regge mechanism, which dominates for higher rapidity and low transverse momenta and is likely to be measured at the LHC by the so-called zero-degree calorimeter. The study was extended to include another new mechanism, where an exchange of two gluons occurs in the t -channel, *i.e.* between the incoming and outgoing photons, Ref. [34]. The analysis was also extended for the case of proton-proton collisions. Another study, Ref. [35], which were performed in collaboration with members of the ALICE and LHCb group, is closely related to the acceptance of a given experiment. Theoretical predictions show the possibility to pioneer the measurement of two photons in the invariant mass region, which has not been experimentally achievable so far. Below the value of $M_{\gamma\gamma} = 2$ GeV, the background coming from two neutral pions which decay into four photons, never considered in the context of light-by-light scattering, is taken into account. The performed analysis takes into account the case when one of the measurable photons comes from the first pion and the second photon from the second pion. The other two photons do not fall into the detection range. Although the pion background, after taking experimental constraints into account, is one order of magnitude larger than the fermion signal, in the invariant mass range below 2 GeV, it becomes crucial to include resonances that decay into two photons. Predictions (made for the first time in the world) show that the resonance contributions η and η' have a good chance of being measured by the ALICE and

LHCb experiments. The results are considered as a strong point for future measurements of the $PbPb \rightarrow PbPb\gamma\gamma$ process.

The electromagnetic production of two electron-positron pairs, Ref. [41], was preceded by a verification of the correctness of the used model for the lowest order QED $\gamma\gamma \rightarrow e^+e^-$ subprocess in ultraperipheral collisions of lead nuclei. The good agreement of theoretical results with ALICE experimental data for the distribution in the invariant mass of a single pair, became the premise for using EPA to determine the cross sections for the production of e^+e^- two pairs from the double scattering mechanism in UPC. Imposing the kinematic constraints dictated by the ATLAS experiment for the main detector, assuming a total luminosity of $L = 1 \text{ nb}^{-1}$, gives a prediction of the observation of 235 events. The calculations show that the distribution of the difference in rapidity of two of the four produced leptons is clearly broader for particles of the same sign regardless of the constraint on the transverse momentum. Results are also presented for the pionic background, which

decreases with increasing kinematic cut on transverse momentum. The rareness of the calculation methodology used, which provides a series of differential cross sections that are a key source of information for the experimental measurement, leads to the possibility of presenting predictions by variable selection. Investigations of production of four leptons were extended by analysis for muon pairs, Ref. [51], taking into account direct creation of the state $\mu^+\mu^-\mu^+\mu^-$ from $\gamma\gamma$ fusion. An unbeatable result turns out for production of two pairs of muons through mechanism of double scattering, $\sigma_{A_1A_2 \rightarrow A_1A_2(\mu^+\mu^-)(\mu^+\mu^-)} / \sigma_{A_1A_2 \rightarrow A_1A_2\mu^+\mu^-\mu^+\mu^-} \approx (10^2 - 10^3)$. The cross section for the one pair muon production in the UPC is also several orders of magnitude larger: $\sigma_{A_1A_2 \rightarrow A_1A_2\mu^+\mu^-} / \sigma_{A_1A_2 \rightarrow A_1A_2(\mu^+\mu^-)(\mu^+\mu^-)} \approx (10^2 - 10^3)$. This type of combination of cross sections, taking into account also distributions in transverse momentum, rapidity or difference $y_{diff} = y_{\ell^\pm} - y_{\ell^\pm}$, represents the first physical analysis to present elementary and nuclear distribution in detail.

-
- i.* Run3 is planned to start in 2029.
- ii.* It is more correct to operate with the notation of pseudorapidity. It was verified that for massless particles the equation $\eta = y$ is fulfilling. For light particles (as for example electrons) with a very good approximation it is possible to apply the limitation on the rapidity instead of pseudorapidity.
1. C. A. Bertulani and G. Baur, Electromagnetic Processes in Relativistic Heavy Ion Collisions, *Phys. Rept.* **163** (1988) 299, [https://doi.org/10.1016/0370-1573\(88\)90142-1](https://doi.org/10.1016/0370-1573(88)90142-1).
 2. C. A. Bertulani, S. R. Klein, and J. Nystrand, Physics of ultraperipheral nuclear collisions, *Ann. Rev. Nucl. Part. Sci.* **55** (2005) 271, <https://doi.org/10.1146/annurev.nucl.55.090704.151526>.
 3. A. Baltz *et al.*, The Physics of ultraperipheral collisions at the LHC, *Phys. Rept.* **458** (2008) 1, <https://doi.org/10.1016/j.physrep.2007.12.001>.
 4. E. Fermi, On the Theory of the impact between atoms and electrically charged particles, *Z. Phys.* **29** (1924) 315, <https://doi.org/10.1007/BF03184853>.
 5. C. F. von Weizsacker, Radiation emitted in collisions of very fast electrons, *Z. Phys.* **88** (1934) 612, <https://doi.org/10.1007/BF01333110>.
 6. E. J. Williams, Nature of the high-energy particles of penetrating radiation and status of ionization and radiation formulae, *Phys. Rev.* **45** (1934) 729, <https://doi.org/10.1103/PhysRev.45.729>.
 7. M. Klusek, W. Schäfer, and A. Szczurek, Exclusive production of $\rho^0\rho^0$ pairs in $\gamma\gamma$ collisions at RHIC, *Phys. Lett. B* **674** (2009) 92, <https://doi.org/10.1016/j.physletb.2009.03.006>.
 8. G. Baur *et al.*, Coherent $\gamma\gamma$ and γ -A interactions in very peripheral collisions at relativistic ion colliders, *Phys. Rept.* **364** (2002) 359, [https://doi.org/10.1016/S0370-1573\(01\)00101-6](https://doi.org/10.1016/S0370-1573(01)00101-6).
 9. H. De Vries, C. W. De Jager, and C. De Vries, Nuclear charge and magnetization density distribution parameters from elastic electron scattering, *Atom. Data Nucl. Data Tabl.* **36** (1987) 495, [https://doi.org/10.1016/0092-640X\(87\)90013-1](https://doi.org/10.1016/0092-640X(87)90013-1).
 10. O. Halpern, Scattering processes produced by electrons in negative energy states, *Phys. Rev.* **44** (1933) 855, <https://doi.org/10.1103/PhysRev.44.855.2>.
 11. W. Heisenberg and H. Euler, Consequences of Dirac's theory of positrons, *Z. Phys.* **98** (1936) 714, <https://doi.org/10.1007/BF01343663>.
 12. M. Böhm and R. Schuster, Scattering of light by light in the electroweak standard model, *Z. Phys. C* **63** (1994) 219, <https://doi.org/10.1007/BF01411013>.
 13. G. Jikia and A. Tkabladze, Photon-photon scattering at the photon linear collider, *Phys. Lett. B* **323** (1994) 453, [https://doi.org/10.1016/0370-2693\(94\)91246-7](https://doi.org/10.1016/0370-2693(94)91246-7).
 14. Z. Bern *et al.*, QCD and QED corrections to light by light scattering, *JHEP* **2001** (2001) 031, <https://doi.org/10.1088/1126-6708/2001/11/031>.
 15. T. Hahn and M. Pérez-Victoria, Automatized one loop calculations in four dimensions and D dimensions, *Comput. Phys. Commun.* **118** (1999) 153, [https://doi.org/10.1016/S0010-4655\(98\)00173-8](https://doi.org/10.1016/S0010-4655(98)00173-8).
 16. G. J. van Oldenborgh and J. A. M. Vermaseren, New Algorithms for One Loop Integrals, *Z. Phys. C* **46** (1990) 425, <https://doi.org/10.1007/BF01621031>.

17. D. Bardin, L. Kalinovskaya, and E. Uglov, Standard Model light-by-light scattering in SANC: analytic and numeric evaluation, *Phys. Atom. Nucl.* **73** (2010) 1878, <https://doi.org/10.1134/S10637788101110098>.
18. P. Lebedowicz, R. Pasechnik, and A. Szczurek, Search for technipions in exclusive production of diphotons with large invariant masses at the LHC, *Nucl. Phys. B* **881** (2014) 288, <https://doi.org/10.1016/j.nuclphysb.2014.02.008>.
19. M. Klusek-Gawenda, P. Lebedowicz, and A. Szczurek, Light-by-light scattering in ultraperipheral Pb-Pb collisions at energies available at the CERN Large Hadron Collider, *Phys. Rev. C* **93** (2016) 044907, <https://doi.org/10.1103/PhysRevC.93.044907>.
20. A. Donnachie and P. V. Landshoff, Total cross-sections, *Phys. Lett. B* **296** (1992) 227, [https://doi.org/10.1016/0370-2693\(92\)90832-0](https://doi.org/10.1016/0370-2693(92)90832-0).
21. A. Donnachie *et al.*, Pomeron physics and QCD, *Camb. Monogr. Part. Phys. Nucl. Phys. Cosmol.* **19** (2002) 1.
22. A. Szczurek, N. N. Nikolaev, and J. Speth, From soft to hard regime in elastic pion-pion scattering above resonances, *Phys. Rev. C* **66** (2002) 055206, <https://doi.org/10.1103/PhysRevC.66.055206>.
23. M. Klusek-Gawenda, W. Schäfer, and A. Szczurek, Two-gluon exchange contribution to elastic $\gamma\gamma \rightarrow \gamma\gamma$ scattering and production of two-photons in ultraperipheral ultrarelativistic heavy ion and proton-proton collisions, *Phys. Lett. B* **761** (2016) 399, <https://doi.org/10.1016/j.physletb.2016.08.059>.
24. H. Cheng and T. T. Wu, Photon-photon scattering close to the forward direction, *Phys. Rev. D* **1** (1970) 3414, <https://doi.org/10.1103/PhysRevD.1.3414>.
25. V. M. Budnev *et al.*, The Two photon particle production mechanism. Physical problems. Applications. Equivalent photon approximation, *Phys. Rept.* **15** (1975) 181, [https://doi.org/10.1016/0370-1573\(75\)90009-5](https://doi.org/10.1016/0370-1573(75)90009-5).
26. P. Lebedowicz and A. Szczurek, The role of meson exchanges in light-by-light scattering, *Phys. Lett. B* **772** (2017) 330, <https://doi.org/10.1016/j.physletb.2017.06.060>.
27. M. Aaboud *et al.*, Evidence for light-by-light scattering in heavy-ion collisions with the ATLAS detector at the LHC, *Nature Phys.* **13** (2017) 852, <https://doi.org/10.1038/nphys4208>.
28. H. Euler, On the scattering of light by light according to Dirac's theory, *Annalen Phys.* **26** (1936) 398, <https://doi.org/10.1002/andp.19364180503>.
29. G. Aad *et al.*, Observation of light-by-light scattering in ultraperipheral Pb+Pb collisions with the ATLAS detector, *Phys. Rev. Lett.* **123** (2019) 052001, <https://doi.org/10.1103/PhysRevLett.123.052001>.
30. A. Sirunyan *et al.*, Evidence for light-by-light scattering and searches for axion-like particles in ultraperipheral PbPb collisions at $\sqrt{sNN} = 5.02$ TeV, *Phys. Lett. B* **797** (2019) 134826, <https://doi.org/10.1016/j.physletb.2019.134826>.
31. G. Aad *et al.*, Erratum to: Measurement of light-by-light scattering and search for axion-like particles with 2.2 nb⁻¹ of Pb+Pb data with the ATLAS detector, *JHEP* **2021** (2021) 050, [https://doi.org/10.1007/JHEP11\(2021\)050](https://doi.org/10.1007/JHEP11(2021)050).
32. M. Klusek-Gawenda and A. Szczurek, $\pi^+\pi^-$ and $\pi^0\pi^0$ pair production in photon-photon and in ultraperipheral ultrarelativistic heavy-ion collisions, *Phys. Rev. C* **87** (2013) 054908, <https://doi.org/10.1103/PhysRevC.87.054908>.
33. C. Patrignani *et al.*, Review of Particle Physics, *Chin. Phys. C* **40** (2016) 100001, <https://doi.org/10.1088/1674-1137/40/10/100001>.
34. M. Klusek-Gawenda *et al.*, Light-by-light scattering in ultraperipheral heavy-ion collisions at low diphoton masses, *Phys. Rev. D* **99** (2019) 093013, <https://doi.org/10.1103/PhysRevD.99.093013>.
35. S. Uehara *et al.*, High-statistics study of neutral-pion pair production in two-photon collisions, *Phys. Rev. D* **79** (2009) 052009, <https://doi.org/10.1103/PhysRevD.79.052009>.
36. H. Marsiske *et al.*, A Measurement of $\pi^0\pi^0$ Production in Two Photon Collisions, *Phys. Rev. D* **41** (1990) 3324, <https://doi.org/10.1103/PhysRevD.41.3324>.
37. B. B. Abelev *et al.*, Performance of the ALICE Experiment at the CERN LHC, *Int. J. Mod. Phys. A* **29** (2014) 1430044, <https://doi.org/10.1142/S0217751X14300440>.
38. M. Williams, M. Bellis, and C. A. Meyer, Multivariate sideband subtraction using probabilistic event weights, *JINST* **4** (2009) P10003, <https://doi.org/10.1088/1748-0221/4/10/P10003>.
39. Z. Citron *et al.*, Report from Working Group 5: Future physics opportunities for high-density QCD at the LHC with heavy-ion and proton beams, *CERN Yellow Rep. Monogr.* **7** (2019) 1159, <https://doi.org/10.23731/CYRM-2019-007.1159>.
40. A. N. Artemyev, V. G. Serbo, and A. Surzhykov, Double lepton pair production with electron capture in relativistic heavy-ion collisions, *Eur. Phys. J. C* **74** (2014) 2829, <https://doi.org/10.1140/epjc/s10052-014-2829-z>.
41. M. Klusek-Gawenda and A. Szczurek, Double scattering production of two positron-electron pairs in ultraperipheral heavyion collisions, *Phys. Lett. B* **763** (2016) 416, <https://doi.org/10.1016/j.physletb.2016.10.079>.
42. E. Abbas *et al.*, Charmonium and e^+e^- pair photoproduction at mid-rapidity in ultra-peripheral Pb-Pb collisions at $\sqrt{sNN} = 2.76$ TeV, *Eur. Phys. J. C* **73** (2013) 2617, <https://doi.org/10.1140/epjc/s10052-013-2617-1>.
43. B. Segev and J. C. Wells, A Light fronts approach to electron - positron pair production in ultrarelativistic heavy ion collisions, *Phys. Rev. A* **57** (1998) 1849, <https://doi.org/10.1103/PhysRevA.57.1849>.
44. D. Y. Ivanov, A. Schiller, and V. G. Serbo, Large Coulomb corrections to the e^+e^- pair production at relativistic heavy ion colliders, *Phys. Lett. B* **454** (1999) 155, [https://doi.org/10.1016/S0370-2693\(99\)00323-8](https://doi.org/10.1016/S0370-2693(99)00323-8).

45. R. N. Lee and A. I. Milstein, Coulomb corrections to the $e^+ e^-$ pair production in ultrarelativistic heavy ion collisions, *Phys. Rev. A* **61** (2000) 032103, <https://doi.org/10.1103/PhysRevA.61.032103>.
46. U. Eichmann, J. Reinhardt, and W. Greiner, Crossing symmetry in the high-energy limit and pair production in ultrarelativistic heavy-ion collisions, *Phys. Rev. A* **61** (2000) 062710, <https://doi.org/10.1103/PhysRevA.61.062710>.
47. S. R. Gevorkyan and E. A. Kuraev, Lepton pair production in relativistic ion collisions to all orders in $Z\alpha$ with logarithmic accuracy, *J. Phys. G: Nucl. Part. Phys.* **29** (2003) 1227, <https://doi.org/10.1088/0954-3899/29/6/320>.
48. E. Bartoš *et al.*, Multiple exchanges in lepton pair production in high-energy heavy ion collisions, *J. Exp. Theor. Phys.* **100** (2005) 645, <https://doi.org/10.1134/1.1926426>.
49. M. Luszczak, R. Maciuła, and A. Szczurek, Production of two $c\bar{c}$ pairs in double-parton scattering, *Phys. Rev. D* **85** (2012) 094034, <https://doi.org/10.1103/PhysRevD.85.094034>.
50. M. Klusek-Gawenda and A. Szczurek, Double-scattering mechanism in the exclusive $AA \rightarrow AA\rho^0\rho^0$ reaction in ultrarelativistic collisions, *Phys. Rev. C* **89** (2014) 024912, <https://doi.org/10.1103/PhysRevC.89.024912>.
51. A. van Hameren, M. Klusek-Gawenda, and A. Szczurek, Single- and double-scattering production of four muons in ultraperipheral PbPb collisions at the Large Hadron Collider, *Phys. Lett. B* **776** (2018) 84, <https://doi.org/10.1016/j.physletb.2017.11.029>.
52. A. van Hameren, KaTie: for parton-level event generation with kT-dependent initial states (2016).
53. M. Bury and A. van Hameren, Numerical evaluation of multigluon amplitudes for High Energy Factorization, *Comput. Phys. Commun.* **196** (2015) 592, <https://doi.org/10.1016/j.cpc.2015.06.023>.
54. G. Aad *et al.*, Exclusive dimuon production in ultraperipheral Pb+Pb collisions at $\sqrt{sNN} = 5.02$ TeV with ATLAS, *Phys. Rev. C* **104** (2021) 024906, <https://doi.org/10.1103/PhysRevC.104.024906>.
55. J. Allen *et al.*, Performance of prototypes for the ALICE electromagnetic calorimeter, *Nucl. Instrum. Meth. A* **615** (2010) 6, <https://doi.org/10.1016/j.nima.2009.12.061>.
56. M. Clemencic, *et al.*, The LHCb simulation application, Gauss: Design, evolution and experience, *J. Phys. Conf. Ser.* **331** (2011) 032023, <https://doi.org/10.1088/1742-6596/331/3/032023>.